

Three-Component Functional Additive in a LiPF_6 -Based Carbonate Electrolyte for a High-Voltage LiCoO_2 /Graphite Battery System

Chunguang Pang,^[a, b] Gaojie Xu,^[b] Weizhong An,^{*,[a]} Guoliang Ding,^[b] Xiaochen Liu,^[b] Jingchao Chai,^[b] Jun Ma,^[b] Haisheng Liu,^[b] and Guanglei Cui^{*,[b]}

The effectiveness of multicomponent functional additives on the performances of lithium ion batteries has received increasing attention. Tris(2*H*-hexafluoroisopropyl) borate (THFPB) additive can totally suppress the appearance of a crystallized complex between LiPF_6 and adiponitrile (ADN). Herein, ADN, THFPB, and cyclohexylbenzene are demonstrated to be an effective three-component functional additive in LiPF_6 -based carbonate electrolyte that improves

the cyclability and rate capabilities of LiCoO_2 /graphite full cells charged to 4.4, 4.45, and 4.5 V, respectively. By systematic characterization, it is demonstrated rationally that, with the help of the three-component functional additive, the electrolyte is stabilized and new types of less resistant, thinner, more protective solid-electrolyte interfaces are constructed simultaneously on the surfaces of both electrodes.

Introduction

As a result of their intrinsic high energy density and long lifespan, rechargeable lithium-ion batteries (LIBs) have been used widely as the main power source in portable electronic devices and are expected to play a prominent role in the field of stationary energy storage systems and electric transportation tools.^[1–5] Currently, to meet the higher energy density requirements of future LIBs, great efforts are being made toward the development of cathodes with higher working voltages and larger specific capacity.^[6–13]

Lithium cobalt oxide (LCO), which has a reversible specific capacity of only approximately 140 mAh g^{-1} (half of its theoretical specific capacity, 274 mAh g^{-1}) at an upper cut-off voltage of 4.2 V, is the most successful cathode material for commercialized LIBs.^[2,13] It is well known that the energy density of LIBs is determined by both the operating voltage and capacity of a cell. Therefore, LCO-based LIBs are anticipated to operate at higher voltages than 4.2 V to obtain an increased capacity. Unfortunately, an increase of the upper cut-off voltage to exceed 4.2 V always leads to a clear deterioration of battery performances (especially cyclability and safety) because of the accelerated interfacial parasitic reactions between the charged LCO electrode and nonaqueous electrolytes. Consequently, unwanted crystal-structure damage/phase transition, Co dissolution–migration–deposition, and electrolyte decomposition occur.^[14,15]

At present, there are two main approaches to improve the interfacial stability between the LCO electrode and nonaqueous electrolytes at elevated cut-off charge voltages. First, the LCO surface can be coated with various materials, such as metal oxides (e.g., Al_2O_3 , MgO , ZnO , ZrO_2),^[16–23] metal phosphates (e.g., AlPO_4),^[24–26] metal fluorides/oxyfluorides (e.g., AlF_3 , ZrO_xF_y),^[27,28] Li ion conductors (e.g., Li_2CO_3 , lithium phosphorus oxynitride, Li_3PO_4 ,

$\text{Li}_{1.3}\text{Al}_{0.3}\text{Ti}_{1.7}(\text{PO}_4)_3$),^[15,29–31] and polymers (e.g., polyimide).^[32] However, it is generally accepted that functional electrolyte additives are of considerable importance in modifying and stabilizing the solid-electrolyte interface (SEI) layer, which determines the cycle life and safety of LIBs significantly.^[8–10,33–39] Hence, the second strategy is the development of new electrolytes for LCO-based cells using functional additives, such as phenyl-containing compounds (e.g., benzenes,^[40–43] anilines,^[43,44] phenyl-containing ether or thioethers^[41,43,45]), heterocyclic compounds (e.g., thiophenes,^[41–43,46,47] furans,^[41,43] pyrroles,^[41] bismaleimide monomers,^[48,49] sulfonates,^[50] cyclic carbonates^[14]), phosphazenes,^[51] boron-based anion receptors,^[52] aliphatic dinitriles,^[53] and inorganic materials (e.g., Al_2O_3 , Li_2CO_3).^[54,55] Actually, most of these functional additives are effective to protect the LCO cathode by participating in the modification of the SEI layer (sometimes forming a conductive polymeric film) to stabilize the electrode-electrolyte interface efficiently by suppressing undesired parasitic reactions.

Aliphatic dinitriles $[\text{NC}-(\text{CH}_2)_n-\text{CN}]$, such as succinonitrile (SN) and adiponitrile (ADN)] are usually used as solvents for high-voltage electrolytes (HVEs) because of their ultra-

[a] C. Pang, Prof. W. An
College of Chemistry and Chemical Engineering, Ocean University of China
Qingdao 266100 (PR China)
E-mail: awzhong@ouc.edu.cn

[b] C. Pang, G. Xu, G. Ding, X. Liu, J. Chai, Dr. J. Ma, H. Liu, Dr. G. Cui
Qingdao Industrial Energy Storage Research Institute, Qingdao Institute of Bioenergy and Bioprocess Technology, Chinese Academy of Sciences
No. 189 Songling Road, 266101 Qingdao (PR China)
Fax: +86-532-80662746
E-mail: cuigl@qibebt.ac.cn

Supporting Information for this article can be found under:
<https://doi.org/10.1002/ente.201700118>.

high electrochemical stability window.^[56] Recently, aliphatic dinitriles (always short-chain SN) were further investigated as thermal-safety-enhancing additives that form a strong complex between the surface transition metal ions and functional nitrile ($-\text{CN}$) groups.^[53,57–61] Boron-based anion receptors, for example, tris(pentafluorophenyl) borane (TPFPB), tris(2*H*-hexafluoroisopropyl) borate (THFPB), and trimethylboroxine (TMB), are of high importance in the formation of protective SEI layers at both the anode and cathode surfaces, especially in high-voltage LIBs.^[52,62–68] As the boron-based anion receptors are stronger Lewis acids than Li^+ and can form donor–acceptor interactions with anions (e.g., PF_6^- , F^- , O_2^{2-} , O_2^-), not only the solubility of various Li compounds (e.g., LiPF_6 , LiF , Li_2O , Li_2O_2) but also the Li^+ transference number increases. Furthermore, the boron-based anion receptors can improve the thermal stability of the LiPF_6 -based electrolyte by the enhancement of $\text{Li}^+ \text{PF}_6^-$ ion-pair dissociation.^[62] Therefore, boron-based anion receptors are normally added as additives to improve both the rate capability and cyclic stability of LIBs. As a typical additive for overcharge protection, a small amount of cyclohexylbenzene (CHB; e.g., 0.1–0.2 wt %) tends to generate a thin electron-conducting protective membrane on the cathode surface.^[36,40,41,69,70] Systematic studies on the influence of multi-component functional additives in electrolytes are of great importance and are urgently needed.^[38,71] In this work, we investigated the synergistic effects of ADN, THFPB, and CHB as three-component functional additive (Figure 1) in LiPF_6 -based carbonate electrolytes for a high-voltage LCO/graphite battery system.

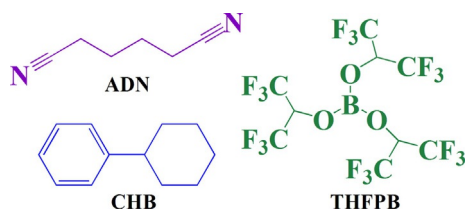


Figure 1. Chemical structures of ADN, THFPB, and CHB.

Results and Discussion

Electrochemical properties of cells with a high-voltage electrolyte containing a three-component functional additive

The addition of the long-chain aliphatic dinitrile ADN (3 wt %) into the basic electrolyte (BE) led inevitably to the appearance of transparent needle-shaped crystals at room temperature (see the video in the Supporting Information). By analysis of the XRD pattern (Figure 2a), we see that the obtained transparent needle-shaped crystal is not the standard LiPF_6 salt. The FTIR spectra of the crystals (rinsed with petroleum ether three times) are mainly comprised of strong characteristic peaks of ADN (2274 and 724 cm^{-1}) and LiPF_6 (851 and 555 cm^{-1} ; Figure 2b). Therefore, we infer that a crystallized complex between ADN and LiPF_6 is formed.^[72] The formation of this crystallized complex will in-

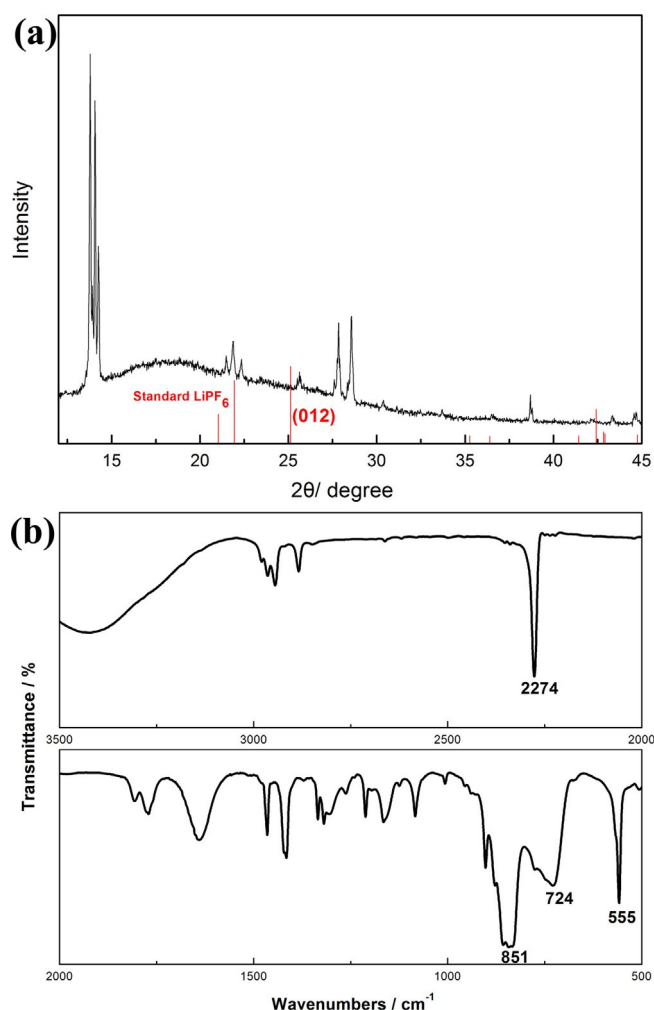


Figure 2. (a) XRD patterns and (b) FTIR spectra of the transparent needle-shaped crystals caused by the addition of only ADN (3 wt %) into BE.

evitably reduce the concentration of LiPF_6 and block the homogeneous migration of Li^+ in the electrolyte. Interestingly, the transparent needle-shaped crystals disappeared after the addition of boron-based anion receptor THFPB. This phenomenon shows that we need to consider combinations based on various long-chain aliphatic dinitriles and boron-based anion receptors as functional additives in LiPF_6 -based carbonate electrolyte for LIBs. The LCO/graphite full cells could not be charged normally (if the potential is ≥ 4.4 V) with the combination of 3 wt % ADN and 1 wt % THFPB. Therefore, 0.1 wt % CHB was added to guarantee normal charge–discharge of the cell by generating a thin electron-conducting protective membrane on the cathode surface at elevated potentials.

The synergistic effects of the ADN–THFPB–CHB additives on the cyclability and rate capabilities of LCO/graphite full cells charged to 4.4, 4.45, and 4.5 V were investigated. Encouragingly, the full cells with HVE show a higher capacity retention of 87.6, 79.6, and 60.0% than their BE-based counterparts at upper cut-off voltages of 4.4, 4.45, and 4.5 V, respectively (Figure 3a–c). Furthermore, upon cycling, the full cells with HVE demonstrate a higher and more stable

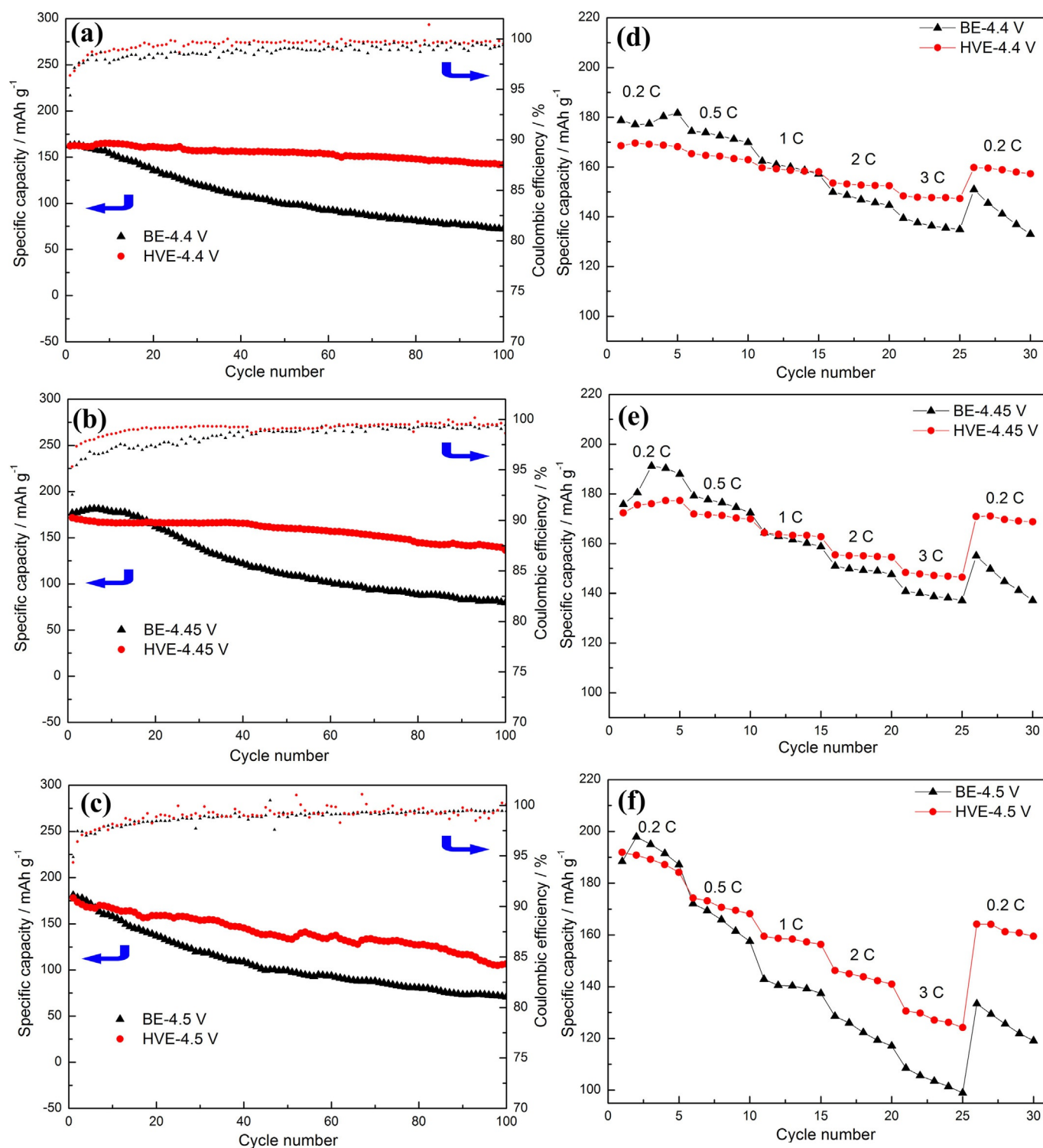


Figure 3. Cyclic and rate performances of LCO/graphite full cells with BE and HVE in the voltage ranges of (a,d) 3.0–4.4 V, (b,e) 3.0–4.45 V, and (c,f) 3.0–4.5 V.

Coulombic efficiency (CE) than their BE-based counterparts. The cyclability of graphite/Li half cells with BE and HVE at 0.1C rate almost show no significant differences over 250 cycles (Figure S1), which indicates that the full cell performances are determined greatly by the behavior of the LCO electrode. Therefore, the enhanced cyclability and CE of the LCO/graphite full cells suggest that the three-component

functional additive offers effective protection for the electrodes (especially the LCO electrode) and alleviate electrolyte decomposition. Full cells with HVE deliver a higher capacity at relatively high discharge rates than their BE-based counterparts (Figure 3d–f), which could be ascribed to the key role of THFPB by augmenting the Li^+ transference number and partially dissolving the resistant components (e.g.,

LiF).^[63,64,68] To understand the modification of the electrode–electrolyte interfaces by the three-component functional additive, the 4.4 V LCO/graphite full cells were studied intensively.

The charge and discharge curves of LCO/graphite full cells (3.0–4.4 V) with BE and HVE for the 1st, 50th, and 100th cycles are shown in Figure 4a and b. Upon cycling, the full-cell capacity deterioration is associated with the ever-increasing electrode polarization (i.e., electrode impedance), which is estimated from the difference between the charge and discharge voltage. By the addition of the functional additive, the electrode polarization becomes much smaller and the voltage plateau is better retained upon cycling. We infer that more favorable electrode surface films are formed with the help of the three-component functional additives. Electrochemical impedance spectroscopy (EIS) was performed to explore the synergistic effects of the three-component functional additive on the electrochemical processes occurring at electrode interfaces. EIS spectra of LCO/graphite full cells (3.0–4.4 V) with BE and HVE at both fully charged and discharged state in the 1st and 100th cycle are presented in Fig-

ure 4c and d. The high-frequency semicircle represents the SEI resistance (R_{SEI}), and the medium-frequency semicircle is attributed to interfacial charge-transfer resistance (R_{CT}). Clearly, regardless of the fully charged (Figure 4c) or fully discharged state (Figure 4d), the LCO/graphite full cells with HVE possess lower interfacial resistances (R_{SEI} and R_{CT}) than their BE-based counterparts at both the 1st and 100th cycle. The reduced R_{SEI} suggests that, in the presence of the three-component functional additive, protective conductive films are formed on both the graphite and LCO electrode surface by suppressing electrolyte decomposition and parasitic reactions, which results in the improved interfacial stability of electrodes and cyclability of full cells. Furthermore, the reduced interfacial resistance is beneficial for the improvement of the rate capability of full cells.

To investigate the effect of the three-component functional additive on the reduction and oxidation behavior of the electrodes, the cyclic voltammograms (CVs) of graphite/Li and LCO/Li half cells at 0.2 mV s^{-1} were measured. In the CV curves, the major anodic peak and cathodic peak denote the Li^+ extraction and insertion process, respectively. The CVs

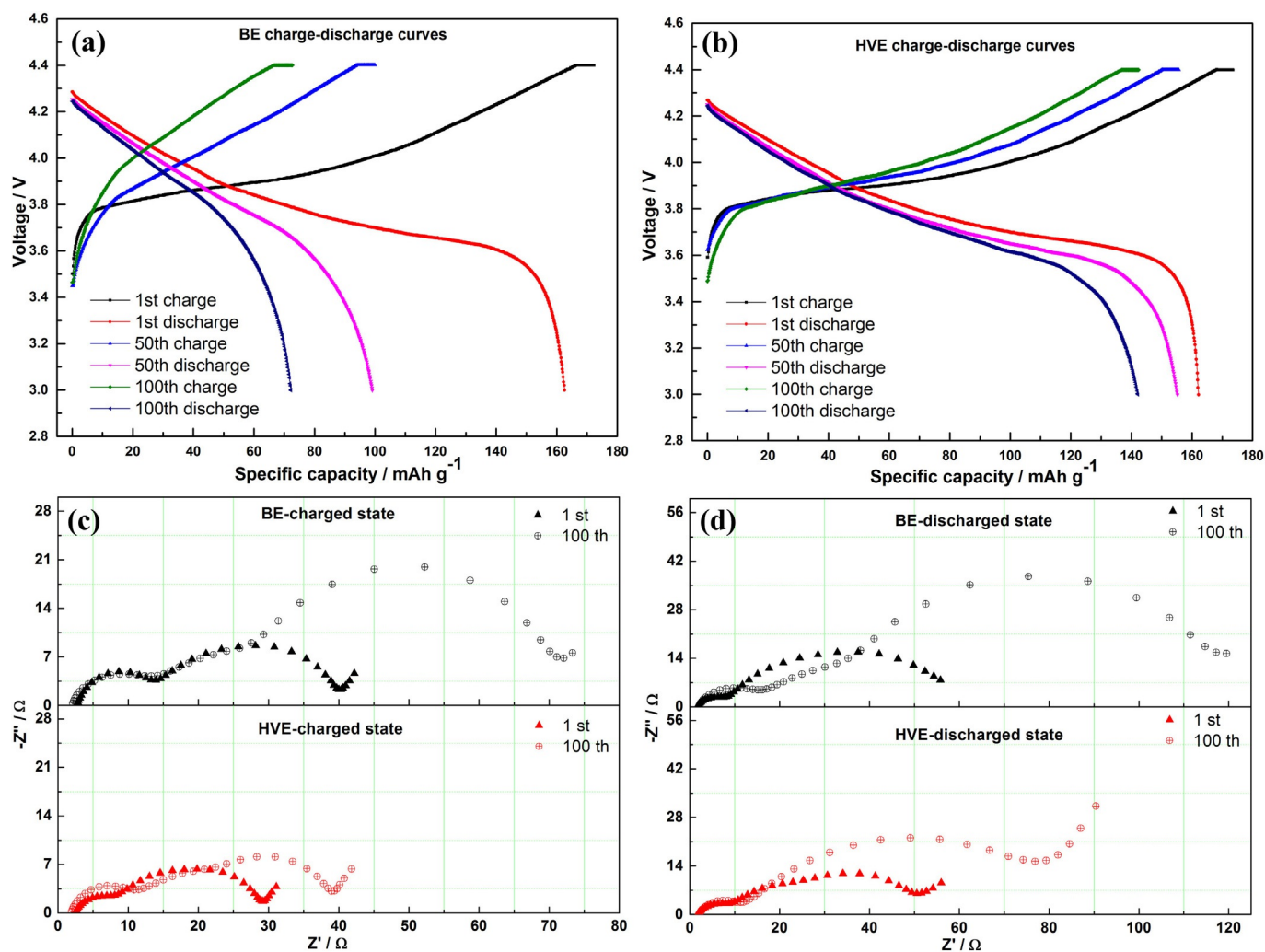


Figure 4. Charge and discharge curves of the LCO/graphite full cells (3.0–4.4 V) with (a) BE and (b) HVE for the 1st, 50th, and 100th cycles. EIS spectra of the LCO/graphite full cells (3.0–4.4 V) with BE and HVE at the (c) fully charged and (d) discharged state of the 1st and 100th cycles.

of graphite/Li (Figure 5a) and LCO/Li (Figure 5b) half cells with BE + 3% ADN show serious polarization, which can be ascribed to the reduced LiPF_6 concentration and blocked homogeneous migration of Li^+ by the formation of a crystallized complex. According to the initial reduction potential of

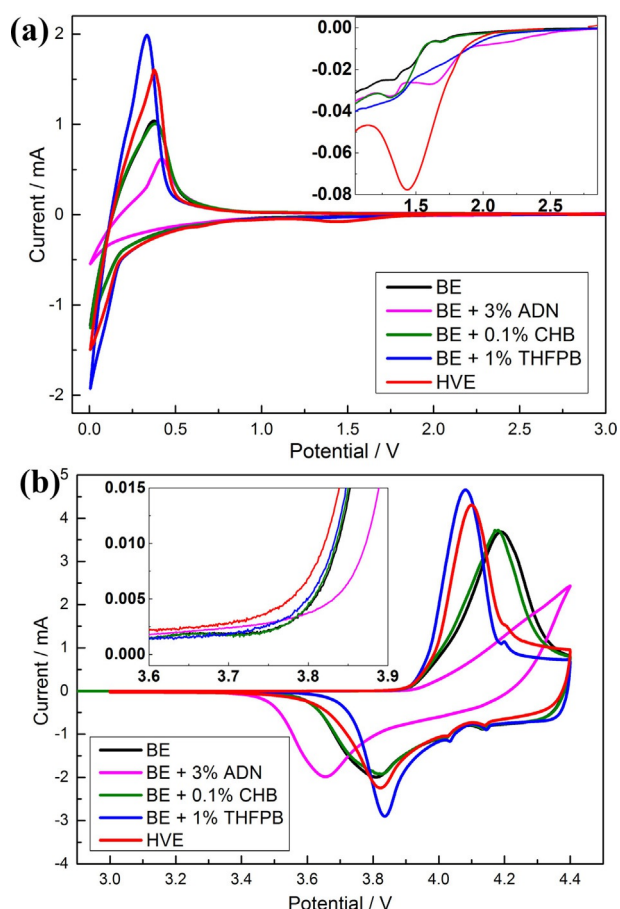


Figure 5. CVs of (a) graphite/Li and (b) LCO/Li half cells with BE, BE + 3 wt% ADN, BE + 0.1 wt% CHB, BE + 1 wt% THFPB, HVE, at 0.2 mVs^{-1} for the first cycle.

the graphite/Li half cell with BE + each single additive, the reduction sequence is ADN, THFPB, and CHB (see inset in Figure 5a). However, the reduction sequence is not distinguishable in the CV of the graphite/Li half cell with HVE, which only shows a strong reduction peak around 1.5 V. This indicates that the three functional additives interact with each other and are reduced preferentially to participate in the SEI formation at the graphite surface. According to the initial oxidation potential of the LCO/Li half cell with BE + each single additive, the oxidation sequence is also ADN, THFPB, and CHB (see inset in Figure 5b). However, the oxidation sequence is also not distinguishable in the CV of the LCO/Li half cell with HVE, which only shows a lower initial oxidation potential than the half cell with BE. This indicates that the ternary functional additives interact with each other and are preferentially oxidized to contribute to the SEI modification at LCO surface.^[52] There are three identical re-

duction peaks at approximately 4.15, 4.05, and 3.83 V for LCO/Li half cells with different electrolytes (except BE + 3 wt% ADN; Figure 5b). A pair of major redox peaks (which contain the reduction peak at approximately 3.82 V) result from the redox reaction of Co^{3+} and Co^{4+} for the first-order phase transformation (Li^+ extraction/insertion) between two hexagonal phases.^[23] Two pairs of minor redox peaks (which contain reduction peaks at approximately 4.15 and 4.05 V, respectively) are caused by the order-disorder phase transformation between hexagonal and monoclinic phases. However, only one oxidation peak is demonstrated for the LCO/Li half cell with BE and BE + 0.1 wt% CHB, which is ascribed to the overlap of the three oxidation peaks. The addition of THFPB additive facilitates the main Li extraction process ($\text{Co}^{3+}/\text{Co}^{4+}$ redox), and one minor oxidation peak appears at approximately 4.2 V (another minor oxidation peak is still overlapped). Furthermore, for both the graphite/Li and LCO/Li half cells, the potential differences between the major anodic and cathodic peaks are smaller because of the addition of the three functional additives (Figure 5a and b). The reduced polarization, which can be mainly ascribed to the key influences of THFPB (Figure 5a and b), also contributes to the enhanced rate capability of the full cells.

Disassembled cell and ex situ characterization

For ex situ characterization, the LCO/graphite full cells with BE and HVE in the voltage ranges of 3.0–4.4 V were disassembled after 100 cycles. For full cells with BE, there are some deep-colored compounds deposited on the separators and stainless steel plate (SS; Figure 6). The elemental contents of the cycled separators (the side close to the graphite electrode) are estimated preliminarily by using energy-dispersive X-ray spectroscopy (EDS; inset of Figure 6). The cycled separator in HVE has higher C and lower O and F contents than the cycled separator in BE. The lower C content of the cycled separator in BE can be attributed to the partial coverage of the polyolefin surface by deep-colored deposits. The lower O and F contents of the cycled separator in HVE suggest that the decomposition of carbonate solvents and LiPF_6 salt are suppressed greatly by the three functional additives. The improved stability of HVE can be ascribed mainly to the increased ion-pair dissociation of the Li^+PF_6^- caused by the boron-based anion receptor of THFPB.^[62]

The surface morphology of the cycled graphite and LCO electrodes disassembled from LCO/graphite full cells with BE and HVE and that of uncycled pristine graphite and LCO electrodes was analyzed by using field-emission scanning electron microscopy (FESEM) and TEM (Figure 7). Pristine graphite particles with a clean surface can be observed (Figure 7a). The surface morphologies of cycled graphite with BE and HVE are very different (Figure 7b and c). After cycling in full cells with BE, a thick and relatively smooth SEI layer is formed on the surface of graphite (Figure 7b). Clearly, some microcracks appear on the SEI layer without additives, indicated by black arrows, which suggests

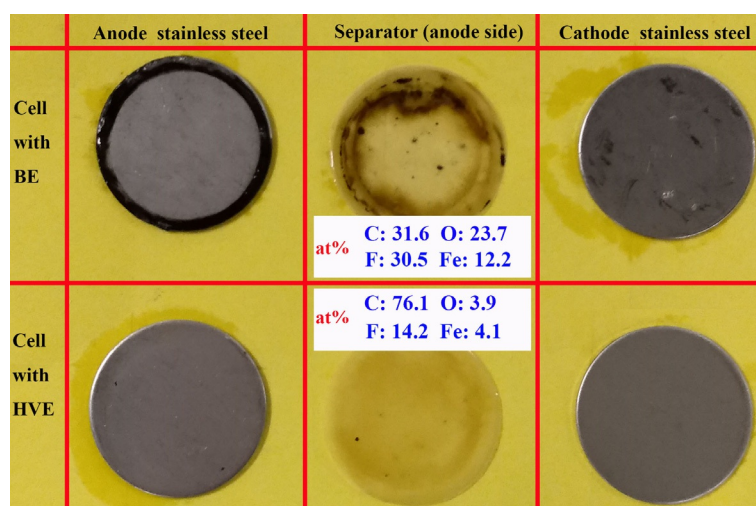


Figure 6. Disassembled LCO/graphite full cells (0.5 C rate, after 100 cycles) with BE and HVE in the voltage ranges of 3.0–4.4 V.

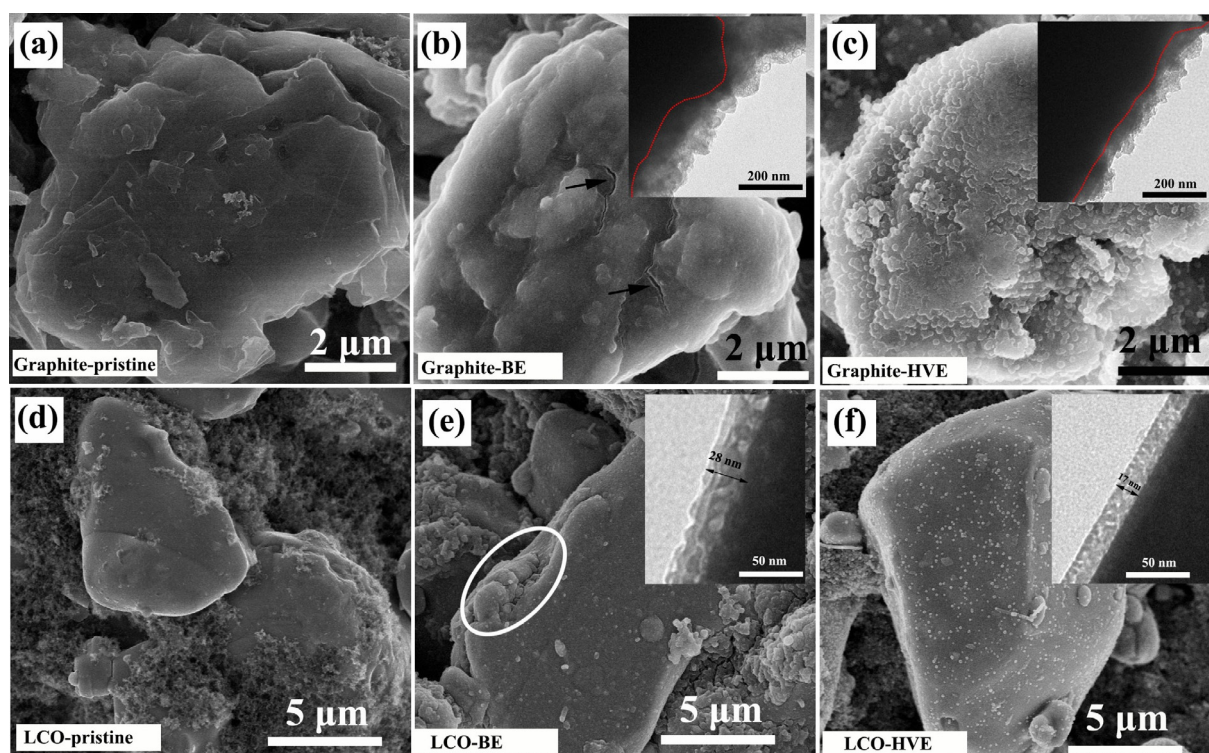


Figure 7. Typical FESEM images of (a) pristine graphite and (d) LCO electrodes, and typical FESEM and TEM images (inset) of cycled graphite and LCO electrodes disassembled from LCO/graphite full cells in voltage ranges of 3.0 V–4.4 V with BE [(b) graphite and (e) LCO] and HVE [(c) graphite and (f) LCO] at 0.5 C rate after 100 cycles.

that the formed SEI is not compact and stable enough for graphite protection. The graphite SEI modified by the three functional additives becomes thinner and much rougher, with large amounts of homogeneous deposits (Figure 7c). For the pristine LCO particle, the surface is clean and smooth (Figure 7d). After LCO is cycled in BE, some significant microcracks (indicated by a white circle in Figure 7e) and macrocracks (indicated by a white circle in Figure S2) appear on the LCO particle. Except for the formation of a thick SEI

layer (≈ 28 nm; inset of Figure 7e) on the surface of LCO cycled in BE, there is also a larger number of large deposits between the LCO particles (enclosed by a white line in Figure S3). For LCO cycled in HVE, there are some deposits distributed uniformly (white points) and no clear macro- or microcracks on the particle surface (Figure 7f). Additionally, the surface of LCO cycled in HVE is covered by a thin (≈ 17 nm) and compact SEI layer (inset of Figure 7f). The XRD patterns of graphite and LCO electrodes disassembled

from the LCO/graphite full cells with BE and HVE are presented in Figure 8. The main (002) peak of the cycled graphite electrode and the main (003) peak of the cycled LCO electrode in HVE display a higher peak intensity and smaller angle shift and peak broadening than their BE-based coun-

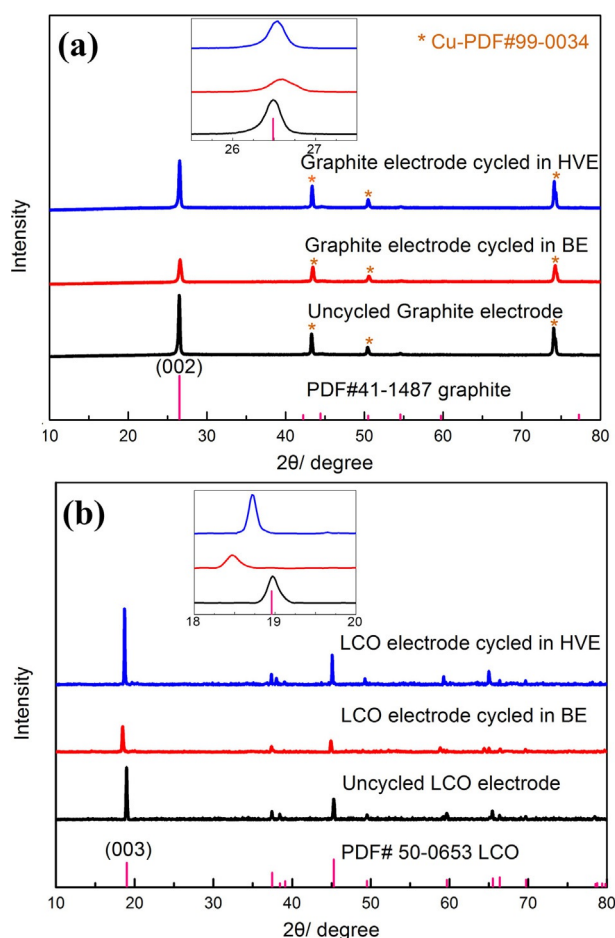


Figure 8. XRD patterns of (a) graphite electrodes and (b) LCO electrodes disassembled from LCO/graphite full cells with BE and HVE at 0.5 C rate after 100 cycles. Inset of (a) is the enlarged (002) diffraction peak of graphite, and inset of (b) is the enlarged (003) diffraction peak of LCO.

terparts, which indicates that the structural degradation of graphite and LCO is suppressed greatly by the addition of the three-component functional additives. In conclusion, new types of thinner, more compact, and protective SEIs for both graphite and LCO electrodes form with the assistance of ADN, THFPB, and CHB functional additives, and consequently, the performances of the LCO/graphite full cells are improved.

To further elucidate the synergistic effects of ternary functional additives on the SEI modifications, the surface compositions of both cycled graphite and LCO electrodes were investigated by using X-ray photoelectron spectroscopy (XPS). Interestingly, both the N and B signals appear on the surface of the cycled graphite and LCO electrodes disassembled from LCO/graphite full cells with HVE, which implies that both ADN and THFPB are incorporated into the surface

SEI during cycling (Figures S4 and S5). All of the peaks in the F1s spectra of the cycled graphite and LCO electrodes with the three-component functional additive show weaker intensities than that of their BE-based counterparts (Figure 9a and b), which indicates that there are less F species in the SEI. For the cycled graphite electrode in BE (Figure 9a), the F1s spectrum mainly contains two peaks, a LiF peak (centered at a binding energy of 684.7 eV) and a $\text{Li}_x\text{PF}_y/\text{PF}_x(\text{OH})_y$ peak (centered at 688.1 eV).^[24–26] Conversely, the F1s spectrum of the cycled graphite electrode in HVE (Figure 9a) only shows one weakened LiF peak (centered at 685.3 eV). For the cycled LCO electrodes in BE (Figure 9b), the F1s spectrum can be deconvoluted into five components centered at 685.3 (LiF, Peak α), 686 (CoF₂, Peak β), 686.6 ($\text{Li}_x\text{PF}_y\text{O}_z$, Peak γ), 687.7 (PVDF (–CF₂), Peak δ), and 688.8 eV ($\text{Li}_x\text{PF}_y/\text{PF}_x(\text{OH})_y$, Peak ϵ).^[24–26] Moreover, the F1s spectrum of the cycled LCO electrode in HVE (Figure 9b) only demonstrates four weakened peaks centered at 684.4 (LiF, Peak α^1), 686 (CoF₂, Peak β^1), 686.7 ($\text{Li}_x\text{PF}_y\text{O}_z$, Peak γ^1), and 687.5 eV (PVDF (–CF₂), Peak δ^1) without peaks related to $\text{Li}_x\text{PF}_y/\text{PF}_x(\text{OH})_y$. We can reasonably infer that the reduced F species in SEI can be attributed to the partial dissolution and enhanced Li^+PF_6^- ion-pair dissociation by the boron-based anion receptor of THFPB.^[52,62–68] Interestingly, the F1s spectrum of the LCO electrode suggests the formation of CoF₂. Particularly for cycled LCO electrodes in both BE and HVE, the Co2p spectra can be deconvoluted into six peaks (Figure 7c and d), LCO Co2p_{3/2} (≈ 780.3 eV, Peak 1) and its satellite (≈ 790.3 eV, Peak 4), LCO Co2p_{1/2} (≈ 795.5 eV, Peak 5) and its satellite (≈ 805.5 eV, Peak 6), and CoF₂ Co2p_{3/2} (≈ 783.7 eV, Peak 2) and its satellite (≈ 788.3 eV, Peak 3).^[24–26] Significantly, the CoF₂ Co2p_{3/2}-related peaks dominate the Co2p spectrum of cycled LCO electrode in HVE, which further confirms the generation of stable, protective, and conductive CoF₂, which can stabilize the SEI layer, suppress electrolyte decomposition, and possibly facilitate the migration of Li^+ .^[24–26,73,74] It is inferred that the formation of CoF₂ originates from the F[–] attack on the surface complex between Co species and ADN. There is a great possibility that these F[–] species originate mainly from the THFPB additive (which contains large amounts of F atoms) rather than from the corrosive HF. Furthermore, FTIR spectra of the cycled LCO electrode were obtained (Figures S6–S9). The weak signals centered at 1597, 1577, 1500, and 1450 cm^{–1} are typical of the C=C stretching of aromatic compounds. Together with the appearance of the C–H bending centered at 758 cm^{–1}, we infer that CHB is polymerized on the surface of LCO electrode.^[70] The stretching of C≡N and the bending vibration of B–O are seen in the spectra at 2244 and 717 cm^{–1},^[52] respectively, which further confirms the participation of ADN and THFPB in SEI modification on the LCO electrode.

We summarized and analyzed all the aforementioned results and illustrated the synergistic effects of the ADN–THFPB–CHB additive in LiPF_6 -based carbonate electrolyte for high-voltage LCO/graphite battery system schematically

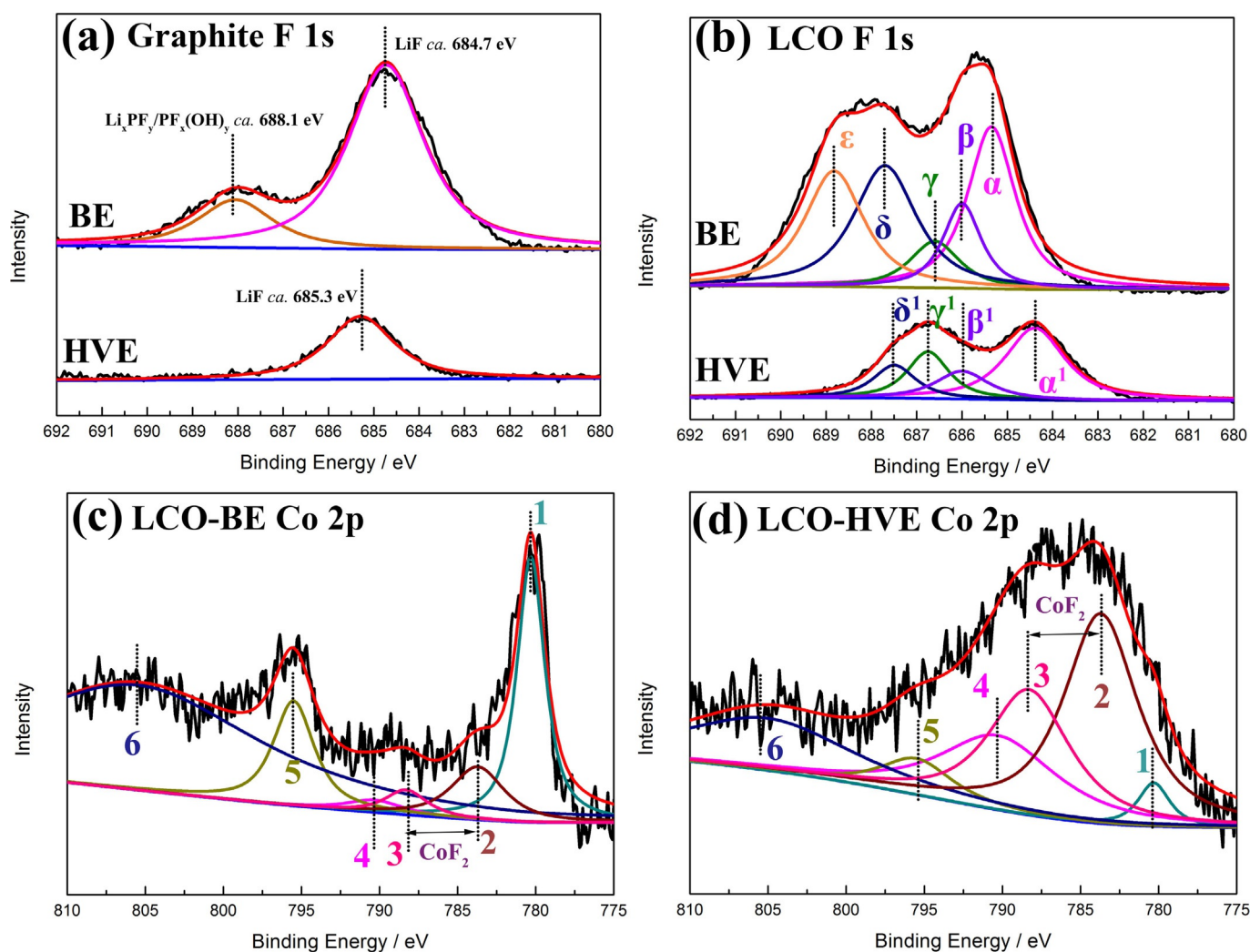
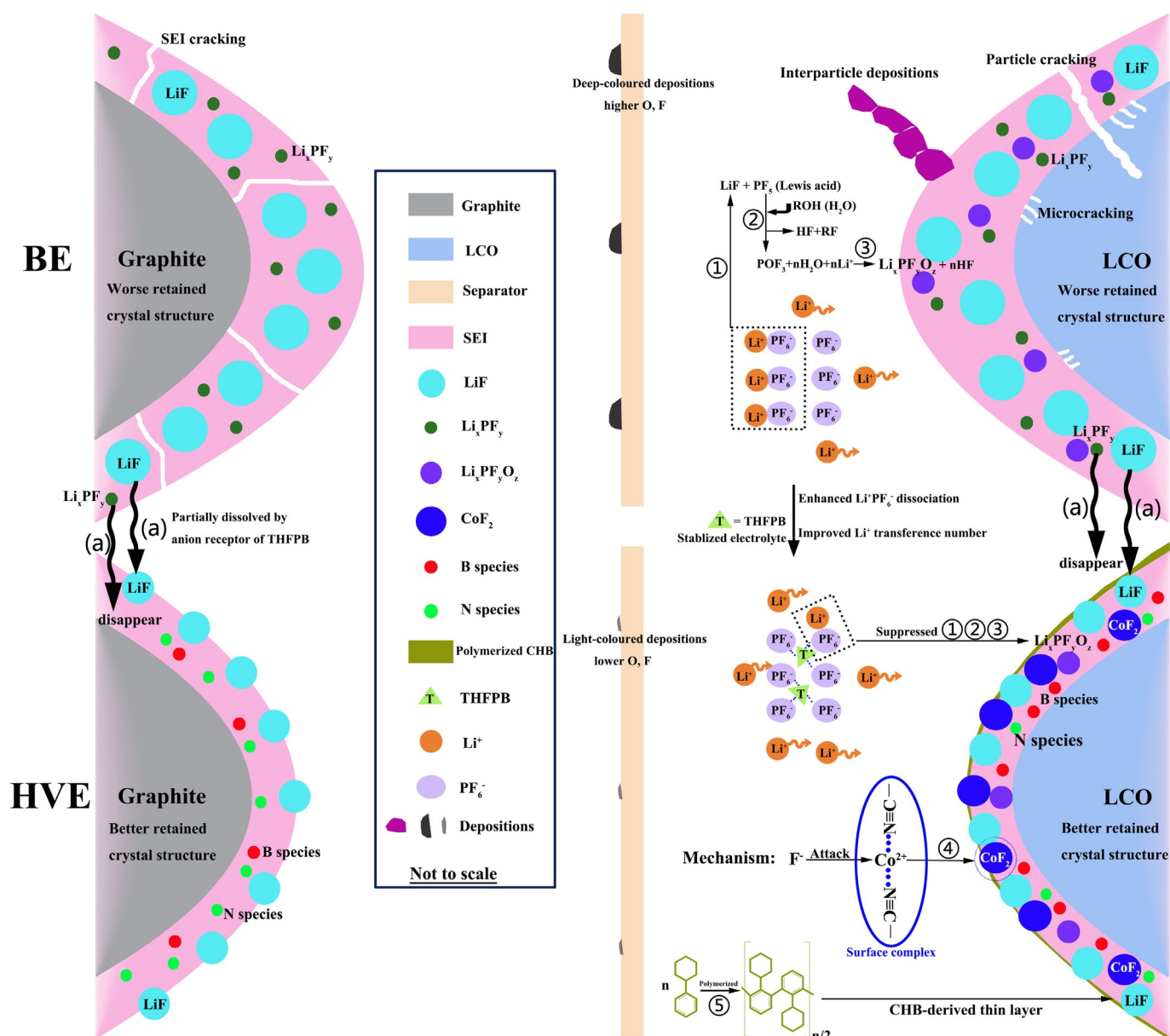


Figure 9. F 1s XPS spectra of (a) the cycled graphite, and the (b) F 1s and (c, d) Co 2p XPS spectra of the cycled LCO electrodes disassembled from LCO/graphite full cells with BE and HVE at 0.5 C rate after 100 cycles.

in Scheme 1. Generally, the electrolyte is stabilized (see suppressed Reactions 1, 2, and 3 in Scheme 1) and new types of less resistant, thinner, more compact and protective SEIs are formed simultaneously on the surfaces of the graphite anode and LCO cathode with the help of a three-component functional additive, and consequently, the cyclability and rate capability of the high-voltage LCO/graphite full cells are improved. We conclude that both ADN- and THFPB-derived species participate in the SEI modifications of both the graphite and LCO electrode. The formation of stable, protective, and conductive CoF_2 in the SEI of the LCO cathode could originate from the F^- attack to the surface complex between Co species and ADN (Reaction 4 in Scheme 1). The reduced F species in SEI, which relates to the reduction of polarization and interfacial resistances, can be attributed to the partial dissolution and enhanced Li^+PF_6^- ion-pair dissociation by the boron-based anion receptor of THFPB.^[52, 62–68] Furthermore, a small amount of CHB participates in the SEI modification of the LCO cathode at elevated voltages possibly by polymerization (Reaction 5 in Scheme 1).^[70]

Conclusions

Adiponitrile (ADN), tris(2*H*-hexafluoroisopropyl) borate (THFPB), and cyclohexylbenzene (CHB) as a three-component functional additive in LiPF_6 -based carbonate electrolytes effectively improve the cyclability and rate capabilities of lithium cobalt oxide (LCO)/graphite full cells charged to 4.4, 4.45, and 4.5 V. It is rationally demonstrated that, because of the three-component functional additives, the electrolyte is stabilized and new types of less resistant, thin, more compact, and protective solid-electrolyte interfaces (SEIs) are constructed simultaneously on the surfaces of the graphite anode and LCO cathode. Interestingly, the SEI of the LCO cathode contains stable, protective, and conductive CoF_2 , which may originate from the F^- attack on the surface complex between Co species and ADN. THFPB plays a key role in the reduction of polarization and interfacial resistances by partially dissolving the resistant components (such as LiF), which increases Li^+PF_6^- ion-pair dissociation and increases the Li^+ transference number. Furthermore, a small



Scheme 1. Illustration of the synergistic effects of ADN-THFPB-CHB functional additives in a LiPF₆-based carbonate electrolyte for a high-voltage LiCoO₂/graphite battery system.

amount of CHB participates in SEI modification of the LCO cathode at elevated voltages possibly by polymerization. Notably, the addition of the boron-based anion receptor THFPB can completely suppress the appearance of transparent needle-shaped crystals (a LiPF_6 and ADN complex) by the addition of the long-chain aliphatic dinitrile of ADN, which encouraged us to pay more attention to combinations based on various long-chain aliphatic dinitriles and boron-based anion receptors as functional additives in LiPF_6 -based carbonate electrolytes for high-voltage Li-ion batteries (LIBs). Finally, we emphasize that a systematic study of the synergistic effects of multicomponent functional additives in electrolytes will open new avenues to develop high-voltage LIBs with excellent performances.

Experimental Section

Preparation of HVE

The BE was 1.0M LiPF₆ in ethylene carbonate (EC)/diethyl carbonate (DEC)/ethyl methyl carbonate (EMC) (1:1:1 by volume; customized from Suzhou Qianmin Chemistry Co. Ltd., China). THFPB [also called boric acid tris(hexafluoroisopropyl) ester] was purchased from TCI, ADN was purchased from Alfa Aesar, and CHB was purchased from Aladdin. All of these reagents were used without further purification. To prepare the HVE, 3 wt % ADN, 1 wt % THFPB, and 0.1 wt % CHB were added into the BE in an Ar-filled glovebox (Mikrouna, China) with the concentrations of moisture and oxygen less than 1 ppm.

Preparation of electrodes and construction of full cells

The cathode consisted of 93 wt % LCO [kindly supplied by Contemporary Amperex Technology Co. Ltd., China (CATL)], 4 wt % conductive carbon (Super PTMLi, TIMCAL), and 3 wt % polyvinylidene difluoride (PVDF, SolefTM 5130) binder. The anode consisted of 93 wt % artificial graphite (CAG-3M, Shanghai Shanshan Tech Co. Ltd., China), 2 wt % Super PTM Li, and 5 wt % aqueous binder (LA133, Chengdu Indigo power sources Co. Ltd., China). The slurries for the cathode (with *N*-methyl-2-pyrrolidinone (NMP) as the solvent) and anode (water as the solvent) were coated, dried, and pressed on Al foil and Cu foil, respectively. Then, the electrodes were punched into disks (cathode disks diameter = 12 mm, anode disks diameter = 14 mm) followed by additional vacuum drying at 120 °C for 8 h before assembly. Finally, in sequence of shell/SS/graphite electrode/Celgard 2500/LCO electrode/SS/leaf spring/shell, 2032 coin-type LCO/graphite full cells with different electrolytes were constructed with N/P values of approximately 1.35 in an Ar-filled glove-box.

Electrochemical measurements

The charge–discharge behavior of the LCO/graphite full cells were measured at RT by using a LAND battery testing system. The currents for testing were calculated based on the LCO cathode material. All the full cells were charged to elevated cut-off voltages (4.4, 4.45, and 4.5 V, respectively) followed by a constant potential (4.4, 4.45, and 4.5 V, respectively) for 5 min and then discharged to 3.0 V. To evaluate the cyclability, the full cells were cycled at 0.2C for the initial two cycles (called the formation process) and then cycled at 0.5C for 100 cycles. The rate capability testing was performed at 0.2C, 0.5C, 1C, 2C, 3C, and then reversed back to 0.2C, successively. The EIS (VMP3, Bio-Logic Science Instruments SAS) of the full cells at both fully charged and discharged state was performed over frequencies ranging from 1 MHz to 100 mHz using a voltage amplitude of 5 mV. CVs (VMP3, Bio-Logic Science Instruments SAS) of graphite/Li and LCO/Li half cells with BE and HVE at 1.0 mV s^{−1} were also obtained.

Ex situ characterization

The cycled graphite electrodes, LCO electrodes, and separators were dismantled carefully from the discharged full cells and rinsed with electronic-grade dimethyl carbonate (DMC; Shenzhen Capchem Technology Co. Ltd., China) to remove the residues, and then they were dried under vacuum for 8 h at RT before analysis. The surface morphologies of the cycled electrodes were characterized by using FESEM (HITACHI S-4800) and TEM (HITACHI H-7650). The elemental contents of the cycled separators were estimated by using EDS by using a HITACHI S-4800 SEM. XPS spectra were acquired by using an ESCALAB220i-XL spectrometer (VG Scientific) with AlK_α radiation with twin anodes at 14 kV × 16 mA. FTIR spectra were acquired by using a Bruker TENSOR 27 spectrometer. XRD patterns of the cycled electrodes were recorded by using a Bruker-AXS Microdiffractometer (D8 ADVANCE) with CuK_α radiation ($\lambda = 1.5406 \text{ \AA}$) from $2\theta = 10^\circ$ – 90° at a scanning speed of 4° min^{-1} . For comparison, the uncycled pristine electrodes were also characterized.

Acknowledgements

This work was supported by the funding from “135” Projects Fund of CAS-QIBET Director Innovation Foundation, Think-Tank Mutual Fund of Qingdao Energy Storage Industry Scientific Research, the Strategic Priority Research Program of the Chinese Academy of Sciences (Grant No. XDA09010105), National Natural Science Foundation of China (No. 51502319, 21473228), and Shandong Provincial Natural Science Foundation (No. ZR2015QZ01, BS2015CL006).

Conflict of interest

The authors declare no conflict of interest.

Keywords: additives • batteries • carbonate electrolytes • high voltage • synergistic effects

- [1] J. M. Tarascon, M. Armand, *Nature* **2001**, 414, 359–367.
- [2] B. Scrosati, J. Garche, *J. Power Sources* **2010**, 195, 2419–2430.
- [3] T. H. Kim, J. S. Park, S. K. Chang, S. Choi, J. H. Ryu, H. K. Song, *Adv. Energy Mater.* **2012**, 2, 860–872.
- [4] S. C. Nagpure, B. Bhushan, S. S. Babu, *J. Electrochem. Soc.* **2013**, 160, A2111–A2154.
- [5] G. J. Xu, Z. H. Liu, C. J. Zhang, G. L. Cui, L. Q. Chen, *J. Mater. Chem. A* **2015**, 3, 4092–4123.
- [6] A. Kraysberg, Y. Ein-Eli, *Adv. Energy Mater.* **2012**, 2, 922–939.
- [7] A. Manthiram, K. Chemelewski, E. S. Lee, *Energy Environ. Sci.* **2014**, 7, 1339–1350.
- [8] S. Tan, Y. J. Ji, Z. R. Zhang, Y. Yang, *ChemPhysChem* **2014**, 15, 1956–1969.
- [9] N. S. Choi, J. G. Han, S. Y. Ha, I. Park, C. K. Back, *RSC Adv.* **2015**, 5, 2732–2748.
- [10] J. H. Kim, N. P. W. Pieczonka, L. Yang, *ChemPhysChem* **2014**, 15, 1940–1954.
- [11] J. Ma, P. Hu, G. L. Cui, L. Q. Chen, *Chem. Mater.* **2016**, 28, 3578–3606.
- [12] J. R. Croy, M. Balasubramanian, K. G. Gallagher, A. K. Burrell, *Acc. Chem. Res.* **2015**, 48, 2813–2821.
- [13] B. Xu, D. N. Qian, Z. Y. Wang, Y. S. Meng, *Mater. Sci. Eng. R* **2012**, 73, 51–65.
- [14] B. Li, Y. Q. Wang, H. B. Lin, J. S. Liu, L. D. Xing, M. Q. Xu, W. S. Li, *Electrochim. Acta* **2014**, 141, 263–270.
- [15] X. Y. Dai, A. J. Zhou, J. Xu, Y. T. Lu, L. P. Wang, C. Fan, J. Z. Li, *J. Phys. Chem. C* **2016**, 120, 422–430.
- [16] Z. X. Wang, L. J. Liu, L. Q. Chen, X. J. Huang, *Solid State Ionics* **2002**, 148, 335–342.
- [17] Z. H. Chen, J. R. Dahn, *Electrochim. Acta* **2004**, 49, 1079–1090.
- [18] Y. S. Jung, A. S. Cavanagh, L. A. Riley, S. H. Kang, A. C. Dillon, M. D. Groner, S. M. George, S. H. Lee, *Adv. Mater.* **2010**, 22, 2172–2176.
- [19] Z. X. Wang, C. Wu, L. J. Liu, F. Wu, L. Q. Chen, X. J. Huang, *J. Electrochem. Soc.* **2002**, 149, A466–A471.
- [20] J. H. Shim, S. Lee, S. S. Park, *Chem. Mater.* **2014**, 26, 2537–2543.
- [21] X. Y. Dai, L. P. Wang, J. Xu, Y. Wang, A. J. Zhou, J. Z. Li, *ACS Appl. Mater. Interfaces* **2014**, 6, 15853–15859.
- [22] Y. Takahashi, S. Tode, A. Kinoshita, H. Fujimoto, I. Nakane, S. Fujitani, *J. Electrochem. Soc.* **2008**, 155, A537–A541.
- [23] a) B. J. Hwang, C. Y. Chen, M. Y. Cheng, R. Santhanam, K. Ragavendran, *J. Power Sources* **2010**, 195, 4255–4265; b) X. F. Li, J. Liu, X. B. Meng, Y. J. Tang, M. N. Banis, J. L. Yang, Y. H. Hu, R. Y. Li, M. Cai, X. L. Sun, *J. Power Sources* **2014**, 247, 57–69.

- [24] A. T. Appapillai, A. N. Mansour, J. Cho, S. H. Yang, *Chem. Mater.* **2007**, *19*, 5748–5757.
- [25] Y. C. Lu, A. N. Mansour, N. Yabuuchi, S. H. Yang, *Chem. Mater.* **2009**, *21*, 4408–4424.
- [26] R. A. Quinlan, Y. C. Lu, D. Kwabi, S. H. Yang, A. N. Mansour, *J. Electrochem. Soc.* **2016**, *163*, A300–A308.
- [27] Y. K. Sun, S. Y. Chong, S. T. Myung, I. Belharouak, K. Amine, *J. Electrochem. Soc.* **2009**, *156*, A1005–A1010.
- [28] Z. G. Wang, Z. X. Wang, H. J. Guo, W. J. Peng, X. H. Li, G. C. Yan, J. X. Wang, *J. Alloys Compd.* **2015**, *621*, 212–219.
- [29] Y. Kim, G. M. Veith, J. Nanda, R. R. Unocic, M. Chi, N. J. Dudney, *Electrochim. Acta* **2011**, *56*, 6573–6580.
- [30] A. J. Zhou, J. Xu, X. Y. Dai, B. Yang, Y. T. Lu, L. P. Wang, C. Fan, J. Z. Li, *J. Power Sources* **2016**, *322*, 10–16.
- [31] J. H. Shim, J. M. Han, J. H. Lee, S. Lee, *ACS Appl. Mater. Interfaces* **2016**, *8*, 12205–12210.
- [32] J. H. Park, J. H. Cho, E. H. Lee, J. M. Kim, S. Y. Lee, *J. Power Sources* **2013**, *244*, 442–449.
- [33] K. Xu, *Chem. Rev.* **2004**, *104*, 4303–4417.
- [34] S. S. Zhang, *J. Power Sources* **2006**, *162*, 1379–1394.
- [35] J. B. Goodenough, Y. Kim, *Chem. Mater.* **2010**, *22*, 587–603.
- [36] K. Xu, *Chem. Rev.* **2014**, *114*, 11503–11618.
- [37] M. Gauthier, T. J. Carney, A. Grimaud, L. Giordano, N. Pour, H. H. Chang, D. P. Fenning, S. F. Lux, O. Paschos, C. Bauer, F. Maglia, S. Lupart, P. Lamp, S. H. Yang, *J. Phys. Chem. Lett.* **2015**, *6*, 4653–4672.
- [38] A. M. Haregewoin, A. S. Wotango, B. J. Hwang, *Energy Environ. Sci.* **2016**, *9*, 1955–1988.
- [39] K. Abe, M. Colera, K. Shimamoto, M. Kondo, K. Miyoshi, *J. Electrochem. Soc.* **2014**, *161*, A863–A870.
- [40] K. Abe, T. Takaya, H. Yoshitake, Y. Ushigoe, M. Yoshio, H. Y. Wang, *Electrochem. Solid-State Lett.* **2004**, *7*, A462–A465.
- [41] K. Abe, Y. Ushigoe, H. Yoshitake, M. Yoshio, *J. Power Sources* **2006**, *153*, 328–335.
- [42] J. A. Choi, S. M. Eo, D. R. MacFarlane, M. Forsyth, E. Cha, D. W. Kim, *J. Power Sources* **2008**, *178*, 832–836.
- [43] T. Takeuchi, T. Kyuna, H. Morimoto, S. I. Tobishima, *J. Power Sources* **2011**, *196*, 2790–2801.
- [44] J. N. Lee, G. B. Han, M. H. Ryou, D. J. Lee, J. Song, J. W. Choi, J. K. Park, *Electrochim. Acta* **2011**, *56*, 5195–5200.
- [45] M. K. Zhao, X. X. Zuo, X. D. Ma, X. Xiao, L. Yu, J. M. Nan, *J. Power Sources* **2016**, *323*, 29–36.
- [46] K. S. Lee, Y. K. Sun, J. Noh, K. S. Song, D. W. Kim, *Electrochem. Commun.* **2009**, *11*, 1900–1903.
- [47] L. Xia, Y. G. Xia, Z. P. Liu, *Electrochim. Acta* **2015**, *151*, 429–436.
- [48] J. P. Yang, P. Zhao, Y. M. Shang, L. Wang, X. M. He, M. Fang, J. L. Wang, *Electrochim. Acta* **2014**, *121*, 264–269.
- [49] J. P. Yang, Y. F. Zhang, P. Zhao, Y. M. Shang, L. Wang, X. M. He, J. L. Wang, *Electrochim. Acta* **2015**, *158*, 202–208.
- [50] X. X. Zuo, C. J. Fan, X. Xiao, J. S. Liu, J. M. Nan, *J. Power Sources* **2012**, *219*, 94–99.
- [51] L. Xia, Y. G. Xia, Z. P. Liu, *J. Power Sources* **2015**, *278*, 190–196.
- [52] X. S. Wang, L. D. Xing, X. L. Liao, X. F. Chen, W. N. Huang, Q. P. Yu, M. Q. Xu, Q. M. Huang, W. S. Li, *Electrochim. Acta* **2015**, *173*, 804–811.
- [53] Y. J. Ji, S. G. Li, G. M. Zhong, Z. R. Zhang, Y. X. Li, M. J. McDonald, Y. Yang, *J. Electrochem. Soc.* **2015**, *162*, A7015–A7023.
- [54] J. Y. Liu, N. Liu, D. T. Liu, Y. Bai, L. H. Shi, Z. X. Wang, L. Q. Chen, V. Hennige, A. Schuch, *J. Electrochem. Soc.* **2007**, *154*, A55–A63.
- [55] B. R. Wu, Y. H. Ren, D. B. Mu, X. J. Liu, G. C. Yang, F. Wu, *RSC Adv.* **2014**, *4*, 10196–10203.
- [56] a) H. Duncan, N. Salem, Y. Abu-Lebdeh, *J. Electrochem. Soc.* **2013**, *160*, A838–A848; b) Y. Abu-Lebdeh, I. Davidson, *J. Electrochem. Soc.* **2009**, *156*, A60–A65; c) Y. Abu-Lebdeh, I. Davidson, *J. Power Sources* **2009**, *189*, 576–579; d) M. Nagahama, N. Hasegawa, S. Okada, *J. Electrochem. Soc.* **2010**, *157*, A748–A752.
- [57] Y. J. Ji, Z. R. Zhang, M. Gao, Y. Li, M. J. McDonald, Y. Yang, *J. Electrochem. Soc.* **2015**, *162*, A774–A780.
- [58] Y. S. Kim, T. H. Kim, H. Lee, H. K. Song, *Energy Environ. Sci.* **2011**, *4*, 4038–4045.
- [59] G. Y. Kim, R. Petibon, J. R. Dahn, *J. Electrochem. Soc.* **2014**, *161*, A506–A512.
- [60] Y. S. Kim, H. Lee, H. K. Song, *ACS Appl. Mater. Interfaces* **2014**, *6*, 8913–8920.
- [61] R. J. Chen, F. Liu, Y. Chen, Y. S. Ye, Y. X. Huang, F. Wu, L. Li, *J. Power Sources* **2016**, *306*, 70–77.
- [62] X. Sun, H. S. Lee, X. Q. Yang, J. McBreen, *Electrochem. Solid-State Lett.* **2002**, *5*, A248–A251.
- [63] Z. H. Chen, K. Amine, *J. Electrochem. Soc.* **2006**, *153*, A1221–A1225.
- [64] Y. M. Lee, Y. G. Lee, Y. M. Kang, K. Y. Cho, *Electrochem. Solid-State Lett.* **2010**, *13*, A55–A58.
- [65] V. P. Reddy, M. Blanco, R. Bugga, *J. Power Sources* **2014**, *247*, 813–820.
- [66] J. M. Zheng, J. Xiao, M. Gu, P. J. Zuo, C. M. Wang, J. G. Zhang, *J. Power Sources* **2014**, *250*, 313–318.
- [67] V. P. Reddy, E. Sinn, N. Hosmane, *J. Organomet. Chem.* **2015**, *798*, 5–12.
- [68] T. Fukutsuka, T. Nakagawa, K. Miyazaki, T. Abe, *J. Power Sources* **2016**, *306*, 753–757.
- [69] M. Q. Xu, L. D. Xing, W. S. Li, X. X. Zuo, D. Shu, G. L. Li, *J. Power Sources* **2008**, *184*, 427–431.
- [70] N. Iwayasu, H. Honbou, T. Horiba, *J. Power Sources* **2011**, *196*, 3881–3886.
- [71] D. Y. Wang, N. N. Sinha, R. Petibon, J. C. Burns, J. R. Dahn, *J. Power Sources* **2014**, *251*, 311–318.
- [72] P. Bonnet, S. Perdrieux, S. G. Schon, US Pat. 5935541 A, **1999**.
- [73] Y. T. Teng, S. S. Pramana, J. F. Ding, T. Wu, R. Yazami, *Electrochim. Acta* **2013**, *107*, 301–312.
- [74] M. J. Armstrong, A. Panneerselvam, C. O'Regan, M. A. Morris, J. D. Holmes, *J. Mater. Chem. A* **2013**, *1*, 10667–10676.

Manuscript received: February 21, 2017

Revised manuscript received: March 20, 2017

Accepted manuscript online: March 29, 2017

Version of record online: July 6, 2017